Journal of Molecular Modeling (2020) 26:199
https://doi.org/10.1007/s00894-020-04425-1

ORIGINAL PAPER

Novel B-C binary fullerenes following the isolated B_4C_3 hexagonal pyramid rule

Miao Yan[1] · Xin-Xin Tian[1] · Ling Pei[1] · Yuan-Yuan Ma[1] · Wen-Yan Zan[1] · Yue-Wen Mu[1] · Si-Dian Li[1]

Received: 1 April 2020 / Accepted: 18 May 2020

Abstract

B-C binary monolayers and fullerenes (borafullerenes) have received considerable attention in recent years. Inspired by the newly reported B_4C_3 semiconducting boron carbide monolayer isovalent to graphene (Tian et al., *Nanoscale*, 2019, 11, 11099), we predict herein at density functional theory level a new class of borafullerenes (**1**–**8**) following the isolated B_4C_3 hexagonal pyramid rule. The spherically aromatic borafullerenes C_{5h} $B_{20}C_{35}$ (**1**), C_5 $B_{20}C_{45}$ (**2**), C_{5h} $B_{20}C_{55}$ (**3**), and C_5 $B_{20}C_{65}$ (**4**) isovalent to C_{50}, C_{60}, C_{70}, and C_{80}, respectively, possess five isolated B_4C_3 hexagonal pyramids evenly distributed on the waist around the C_5 molecular axis, while S_{10} $B_{40}C_{50}$ (**5**), C_5 $B_{40}C_{60}$ (**6**), S_{10} $B_{40}C_{70}$ (**7**), and C_5 $B_{40}C_{80}$ (**8**) encompass ten isolated B_4C_3 pyramids symmetrically distributed on the cage surface. Detailed orbital and bonding analyses indicate that these borafullerenes follow similar σ and π-bonding patterns with their fullerene analogues, with three delocalized 7c-2e π bonds forming a local π-aromatic system over each isolated B_4C_3 hexagonal pyramid. The calculated formation energies of the $(B_4C_3)_nC_{60-6n}$ ($n = 1$–5) series isovalent to C_{60} appear to increase almost linearly with the number of isolated B_4C_3 pyramids in the system. The IR, Raman, and UV-vis spectra of the prototypical $B_{20}C_{45}$ (2) are theoretically simulated to facilitate its future spectral characterization.

Keywords Borafullerenes · Density functional theory · Structures · Bonding · Isolated hexagonal pyramid rule

Introduction

C_{60} has played a pioneering role in nanoscience and nanotechnology ever since its discovery in 1985 [1–3]. One way to enrich the chemistry of fullerene is to substitute carbon atoms in fullerenes with atoms of other elements to form heterofullerenes. With similar atomic size and bonding capacity with carbon, boron and nitrogen serve as typical doping atoms in fullerenes to form borafullerenes and azafullerenes, respectively. Macroscopic syntheses of azafullerenes were realized in 1995 [4, 5]. However, relatively little experimental attention had been paid to borafullerenes before 2013 [6–9]. The first experimental observation of B_nC_{60-n} borafullerenes ($n = 1$–6) in gas phase by laser vaporization was reported in 1991, with boron-doped 70-atom clusters also particularly abundant [6, 7]. A major breakthrough in facile synthesis of $C_{59}B$ borafullerene by atom exchange resulting from exposure of C_{60} to boron vapor was reported in 2013 [9]. Theoretical investigations on carbon-rich borafullerenes include $C_{n-1}B$ ($n = 60$, 180, 240, 420, 540, 720, 780), $B_{12}C_{48}$, and B_nC_{60-n} ($n \leq 12$) [10–17]. Using a numerical atomic orbital density functional theory, Garg et al. suggested that boron atoms in B_nC_{60-n} ($n = 1$–12) distribute themselves in a way that a pentagon ring does not contain more than one B atom and a hexagon not more than two B atoms (at nonadjacent sites) [16]. Mohr and coworkers predicted "patched" structural motifs with boron aggregations which turned out to be much more stable than the "diluted" structures for $B_{12}C_{48}$ and $B_{12}C_{50}$ in 2014 [17]. Our group predicted in 2018 a series of $B_{40}C_n$ ($n = 30$, 40, and 50) borafullerenes with higher boron contents featuring a B_{30} boron double-chain nano-ring at the equator [18]. Utilizing

Electronic supplementary material The online version of this article (https://doi.org/10.1007/s00894-020-04425-1) contains supplementary material, which is available to authorized users.

✉ Xin-Xin Tian
tianxx@sxu.edu.cn

✉ Yue-Wen Mu
ywmu@sxu.edu.cn

✉ Si-Dian Li
lisidian@sxu.edu.cn

[1] Institute of Molecular Science, Key Laboratory of Materials for Energy Conversion and Storage of Shanxi Province, Shanxi University, Taiyuan 030006, People's Republic of China

Published online: 07 July 2020

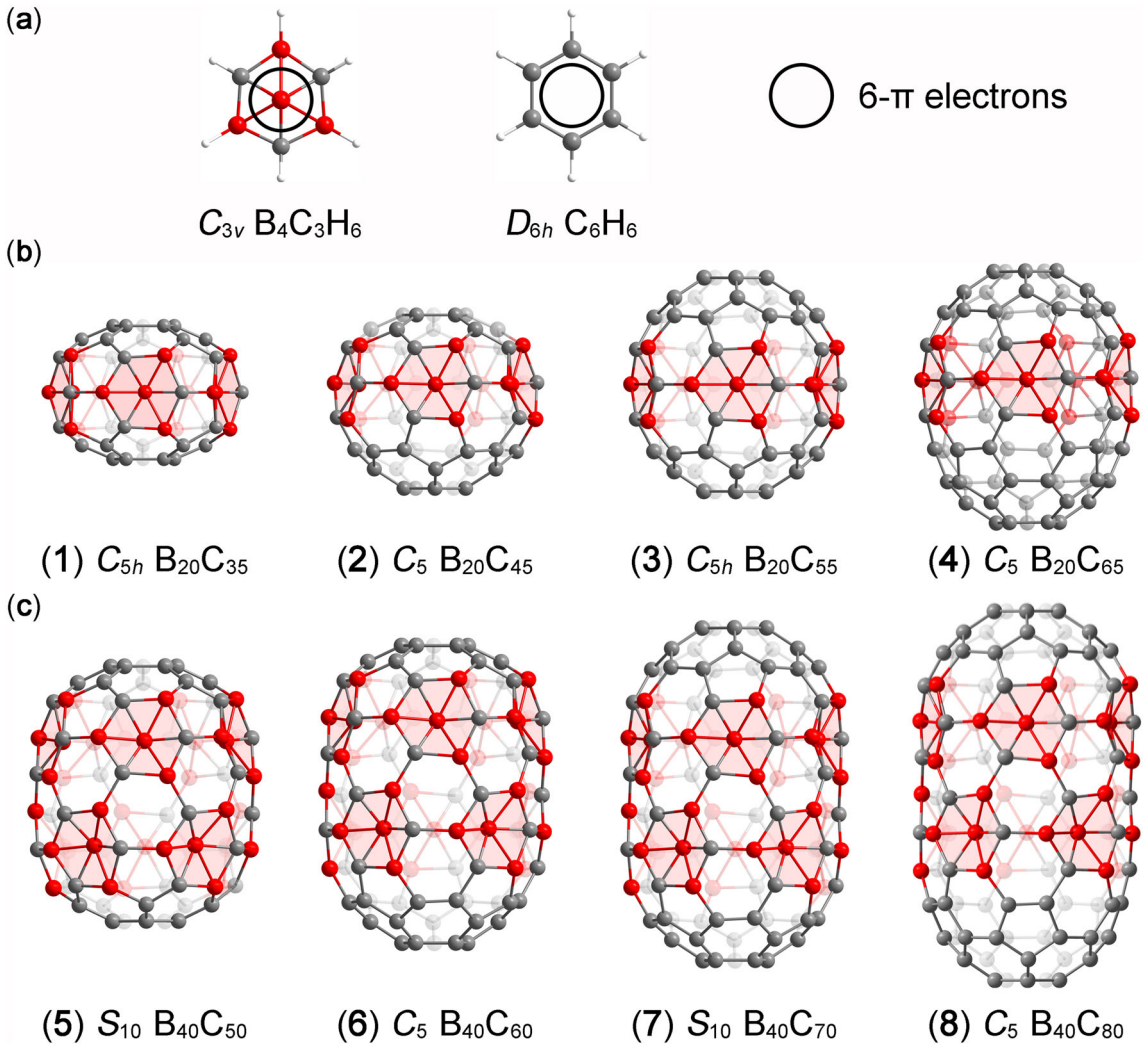

Fig. 1 Structures and delocalized π-bonding patterns of the isovalent C_{3v} $B_4C_3H_6$ and D_{6h} C_6H_6 (**a**) and the optimized structures of C_{5h} $B_{20}C_{35}$ (**1**), C_5 $B_{20}C_{45}$ (**2**), C_{5h} $B_{20}C_{55}$ (**3**), and C_5 $B_{20}C_{65}$ (**4**) at PBE0/6–311 + G(d) level (**b**) and S_{10} $B_{40}C_{50}$ (**5**), C_5 $B_{40}C_{60}$ (**6**), S_{10} $B_{40}C_{70}$ (**7**), and C_5 $B_{40}C_{80}$ (**8**) at PBE0/6–31 + G(d) (**c**), with B atoms in red, C atoms in gray, and H atoms in white

the isovalent relationship between the B-centered C_{3v} $B_4C_3H_6$ and benzene (D_{6h} C_6H_6) (Fig. 1a) which have the same numbers of valence electrons, similar geometrical and electronic structures, and similar π-bonding patterns, we predicted very recently a highly stable B_4C_3 semiconducting boron carbide monolayer ($Pmn2_1$) composed of isolated B_4C_3 hexagonal pyramids with the direct bandgap of 2.73 eV [19]. Such a slightly buckled B_4C_3 boragraphene isovalent to graphene appears to be even more stable than the experimentally synthesized BC_3 monolayer at first-principles theory level, raising the possibility to form a series of stable cage-like borafullerenes isovalent to corresponding fullerenes with isolated B_4C_3 hexagonal pyramids on the cage surface.

Keeping the inspiration in mind, we perform an extensive density functional theory (DFT) investigation in this work on the structures and bonding patterns of a new class of borafullerenes isovalent to their fullerene analogues conforming to the isolated B_4C_3 hexagonal pyramid rule. The obtained C_{5h} $B_{20}C_{35}$ (**1**), C_5 $B_{20}C_{45}$ (**2**), C_{5h} $B_{20}C_{55}$ (**3**), and C_5 $B_{20}C_{65}$ (**4**) (Fig. 1b) feature five isolated B-centered B_4C_3 hexagonal pyramids evenly distributed on the waist, with three delocalized 7c-2e π bonds forming a local π-aromatic system over each isolated B_4C_3 hexagonal pyramid. Bigger borafullerenes S_{10} $B_{40}C_{50}$ (**5**), C_5 $B_{40}C_{60}$ (**6**), S_{10} $B_{40}C_{70}$ (**7**), and C_5 $B_{40}C_{80}$ (**8**) (Fig. 1c) following the same structural and bonding patterns are also predicted.

Methods

The initial high-symmetry C_{5h} $B_{20}C_{35}$ (**1**), C_5 $B_{20}C_{45}$ (**2**), C_{5h} $B_{20}C_{55}$ (**3**), C_5 $B_{20}C_{65}$ (**4**), S_{10} $B_{40}C_{50}$ (**5**), C_5 $B_{40}C_{60}$

(**6**), S_{10} $B_{40}C_{70}$ (**7**), and C_5 $B_{40}C_{80}$ (**8**) were constructed via isovalent substitutions from their fullerene counterparts D_{5h} C_{50}, I_h C_{60}, D_{5h} C_{70}, D_{5d} C_{80}, D_{5d} C_{80}, D_{5h} C_{90}, D_{5d} C_{100}, and D_{5h} C_{110}, respectively. Extensive global searches were performed on the prototypical $B_{20}C_{45}$ ($(B_4C_3)_5C_{30}$) using both the TGMin program [20–22] and minima hoping (MH) method [23, 24], with more than 3000 low-lying stationary points probed on the potential energy surface at PBE level. The low-lying isomers thus obtained were then fully re-optimized at the hybridized DFT-PBE0 level with the basis sets of 6–31 + G(d) and 6–311 + G(d), respectively [25, 26]. The PBE0 functional has been demonstrated to be reliable for boron clusters in comparison with experiments or more accurate ab initio calculations [27–31]. Detailed bonding analyses were performed using the adaptive natural density partitioning (AdNDP) [32–34] method at PBE0/6-31G level. Nucleus-independent chemical shifts [35, 36] were calculated at the cage centers to assess the spherical aromaticity of these borafullerenes. The IR and Raman spectra of $B_{20}C_{45}$ (2) were simulated at PBE0/6–31 + G(d) level and UV-vis absorption spectrum calculated using the time-dependent DFT approach (TD-DFT) [37, 38]. Born–Oppenheimer molecular dynamics (BOMD) simulations were performed on $B_{20}C_{35}$ (**1**), $B_{20}C_{45}$ (**2**), $B_{20}C_{55}$ (**3**), and $B_{20}C_{65}$ (**4**) for 30 ps at 500 K, 800 K, and 1500 K using the CP2K software package [39]. All calculations in this work were performed using the Gaussian 09 package [40].

Results and discussion

Structures and stabilities

We start from B_4C_{57} (I) ($(B_4C_3)C_{54}$) (Fig. 2), the smallest borafullerene concerned in this works. Various isomers in different structural motifs were constructed and compared in Fig. S1. The high-symmetry C_3 B_4C_{57} (I) constructed by isovalent substitution of one C_6 hexagon in I_h C_{60} with a B-filled B_4C_3 hexagonal pyramid (B_4C_3-HP) appears to be the most stable isomer obtained. As a true minimum with the lowest vibrational frequency of $\nu_{min} = 253$ cm^{-1} at PBE0/6–31 + G(d) level, it lies at least 1.43 eV lower than other low-lying isomers (Fig. S1), indicating that the B_4C_3-HP unit with a slightly inward buckled hexa-coordinate B atom at the center (η^6-B) is well maintained in $(B_4C_3)C_{54}$ during structural optimizations due to its unique electronic configuration. Figure 3a indicates that the B-centered quasi-planar C_{3v} $B_4C_3H_6$ possesses three delocalized 7c-2e π bonds over the bowl-shaped B_4C_3-HP framework, similar to the typical π-bonding pattern of benzene (C_6H_6) [19]. Such a bonding pattern renders π aromaticity to C_{3v} $B_4C_3H_6$ (Fig. 1a). The high stability of C_3 $(B_4C_3)C_{54}$ (I) can be understood based on the fact that its formation with respect to $C_{60} + (4B - 3C) = (B_4C_3)C_{54}$ is a $C_6 \rightarrow B_4C_3$ isovalent substitution process from I_h C_{60}. With one more C_6 hexagon in $(B_4C_3)C_{54}$ (I) substituted by a second B_4C_3-HP unit, C_1 $(B_4C_3)_2C_{48}$ (B_8C_{54}) (II) with two isolated

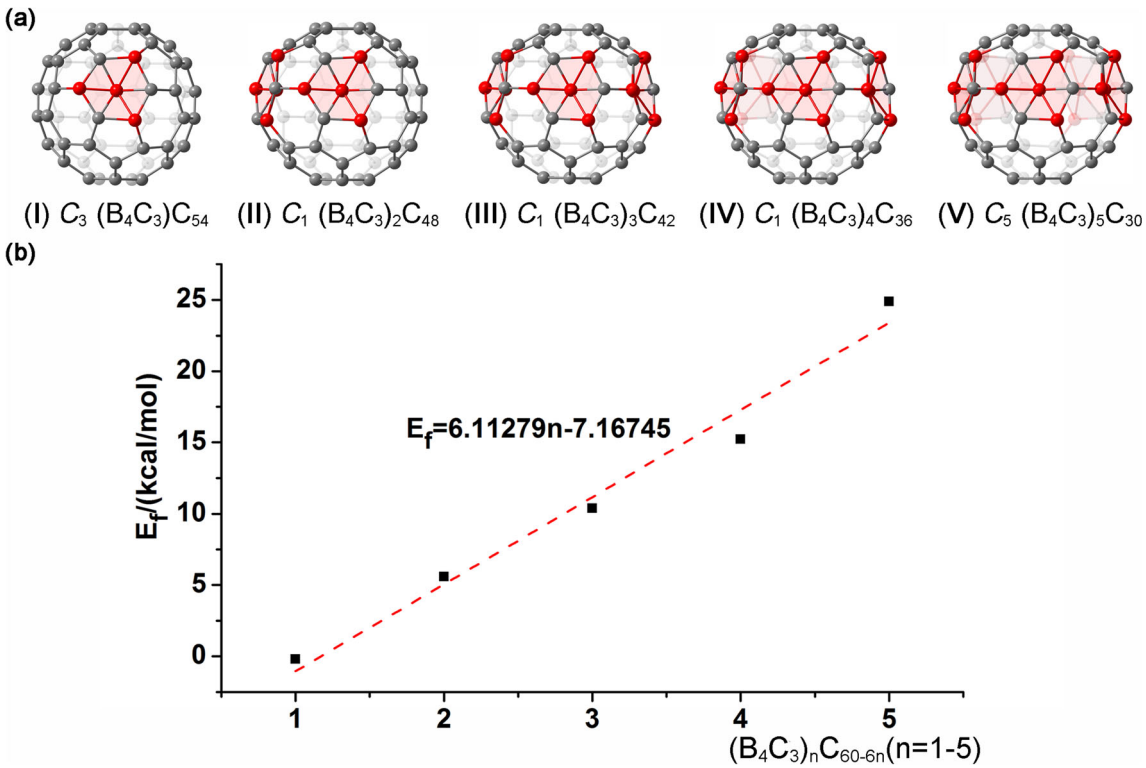

Fig. 2 Optimized structures (**a**) and calculated formation energies of C_3 $(B_4C_3)C_{54}$, C_1 $(B_4C_3)_2C_{48}$, C_1 $(B_4C_3)_3C_{42}$, C_1 $(B_4C_3)_4C_{36}$, and C_5 $(B_4C_3)_5C_{30}$ (**b**) at PBE0/6–31 + G(d) level

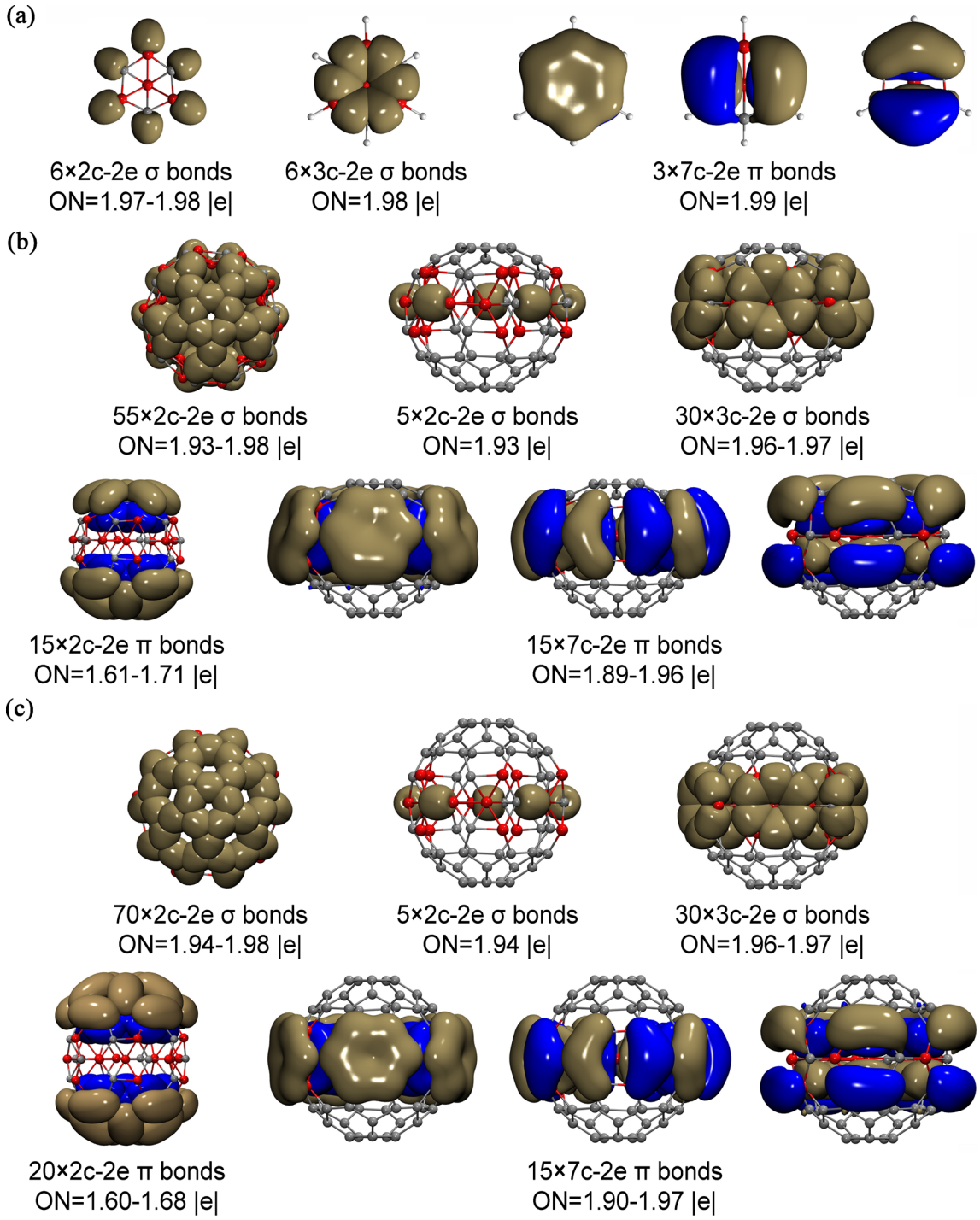

Fig. 3 AdNDP bonding patterns of C_{3v} $B_4C_3H_6$ (**a**), C_5 $B_{20}C_{45}$ (**2**) (**b**), and C_{5h} $B_{20}C_{55}$ (**3**) (**c**), with the occupation numbers (ONs) indicated

B_4C_3-HPs interconnected by a C–B bond turns out to be the most stable isomer obtained lying at least 0.10 eV lower than other low-lying isomers in different structural motifs (Fig. S2), with $\nu_{min} = 241$ cm^{-1}.

More encouragingly, the high-symmetry axially chiral C_5 $B_{20}C_{45}$ (**2**) ($(B_4C_3)_5C_{30}$) constructed by consecutive isovalent substitutions of five C_6 hexagons in C_{60} with five isolated B_4C_3-HP units turned out to be most stable structure obtained in the 3000 isomers probed in this work (Fig. 1b and Fig. S3). C_5 $B_{20}C_{45}$ (**2**) is a true minimum of $B_{20}C_{45}$ with $\nu_{min} = 217$ cm^{-1} though we cannot guarantee that it is the global minimum at this stage because of the extremely complicated potential energy surface of the binary system. It features five isolated B_4C_3-HPs evenly distributed on the waist around the C_5 molecular axis interconnected by five B–C σ bonds between them on the equator, with one bowl-shaped C_{10} cap on

the top and one bowl-shaped C_{20} cap at bottom. It therefore follows the isolated B_4C_3 hexagonal pyramid rule (IHPR), with five equivalent η^6-B atoms located at the centers of five isolated B_4C_3-HPs. As shown in Fig. S3, the second isomer C_1 $B_{20}C_{45}$ with three isolated B_4C_3-HPs on the waist and two isolated B_4C_3-HPs at the bottom with the small relative energy of 0.03 eV is practically iso-energetic with C_5 $B_{20}C_{45}$ (**2**), the third isomer C_1 $B_{20}C_{45}$ with four isolated B_4C_3-HPs on the waist and one isolated B_4C_3-HP at the bottom lies 0.16 eV higher in energy, while all the other low-lying isomers appear to be at least 0.19 eV less stable than $B_{20}C_{45}$ (**2**). Interestingly, all the fifteen lowest-lying isomers of $B_{20}C_{45}$ in different structural motifs within 0.47 eV turned out to conform to the IHPR rule, further indicating the importance of the IHPR rule in these borafullerenes.

Similarly, the high-symmetry borafullerenes C_{5h} $B_{20}C_{35}$ (**1**), C_{5h} $B_{20}C_{55}$ (**3**), C_5 $B_{20}C_{65}$ (**4**) (Fig. 1b), S_{10} $B_{40}C_{50}$ (**5**), C_5 $B_{40}C_{60}$ (**6**), S_{10} $B_{40}C_{70}$ (**7**), and C_5 $B_{40}C_{80}$ (**8**) (Fig. 1c) constructed via consecutive $C_6 \rightarrow B_4C_3$ isovalent substitutions from D_{5h} C_{50}, D_{5h} C_{70}, D_{5d} C_{80}, D_{5d} C_{80}, D_{5h} C_{90}, D_{5d} C_{100}, and D_{5h} C_{110} follow the same IHPR rule, with 5, 5, 5, 10, 10, 10, and 10 isolated B_4C_3-HPs evenly distributed on the waist around the C_5 molecular axis, respectively (Fig. 1). In these borafullerenes, C_5 $B_{20}C_{45}$ (**2**), C_5 $B_{20}C_{65}$ (**4**), C_5 $B_{40}C_{60}$ (**6**), and C_5 $B_{40}C_{80}$ (**8**) belong to typical axially chiral species.

To evaluate the thermodynamical stability of these borafullerenes, we define the formation energy (E_f) of $(B_4C_3)_nC_{60-6n}$ series with respect to $C_{60} + 4nB - 3nC = (B_4C_3)_nC_{60-6n}$ as follows:

$$E_f = -\left[E_{(B4C3)nC60-6n} - (E_{C60} + 4nE_B - 3nE_C)\right]$$

where $E_{(B4C3)nC60-6n}$, E_{C60}, E_B, and E_C are the total energies of $(B_4C_3)_nC_{60-6n}$, C_{60}, B, and C, respectively. As shown in Fig. 2, the formation energies of the $(B_4C_3)_nC_{60-6n}$ ($n = 1$–5) borafullerenes isovalent to C_{60} increase almost linearly with the number of isolated B_4C_3-HPs in the system in an approximate linear relationship of $E_f = 6.11279n - 7.16745$ kcal/mol, suggesting that the isolated B_4C_3-HPs in these clusters can be approximately viewed as independent structural units with weak correlations. The calculated formation energies of **1**–**8** tabulated in Table 1 show that these high-symmetry borafullerenes are generally favored in thermodynamics with respect to their fullerene parent precursors at room temperatures, with certain fluctuations in E_f values depending on specific sizes and shapes of the clusters.

Extensive molecular dynamics (MD) simulations were performed on **1**–**4** for 30 ps at 500 K, 800 K, and 1500 K to check their dynamical stabilities. As shown in Fig. S4, all these borafullerenes are dynamically stable at 1500 K, with the small average root-mean-square-deviations of RMSD = 0.10 Å, 0.09 Å, 0.09 Å, and 0.09 Å and maximum bond length deviations of MAXD = 0.35 Å, 0.33 Å, 0.31 Å, and 0.35 Å for $B_{20}C_{35}$ (**1**), $B_{20}C_{45}$ (**2**), $B_{20}C_{55}$ (**3**), and $B_{20}C_{65}$ (**4**), respectively.

Table 1 Numbers of isolated B_4C_3 hexagonal pyramids (n), HOMO-LUMO gaps (ΔE_{Gap}), NICS values (NICS), and the formation energy (E_f) of the **1**–**8** borafullerenes at PBE0/6–31 + G(d) level

	n	ΔE_{Gaps}/ eV	NICS/ ppm	E_f/ kal mol^{-1}
C_{5h} $B_{20}C_{35}$ (**1**)	5	2.86	− 19	54.78
C_5 $B_{20}C_{45}$ (**2**)	5	3.27	− 16	24.56
C_{5h} $B_{20}C_{55}$ (**3**)	5	3.28	− 22	35.60
C_5 $B_{20}C_{65}$ (**4**)	5	2.38	− 20	11.57
S_{10} $B_{40}C_{50}$ (**5**)	10	3.08	− 16	76.33
C_5 $B_{40}C_{60}$ (**6**)	10	3.28	− 15	64.64
S_{10} $B_{40}C_{70}$ (**7**)	10	3.28	− 13	71.5
C_5 $B_{40}C_{80}$ (**8**)	10	2.43	− 12	33.36

Electronic structures and bonding pattern analyses

The high stabilities of these borafullerenes originate from their unique electronic structures and bonding patterns. As shown in Table 1, **1**–**8** possess considerably large calculated HOMO–LUMO energy gaps, with $\Delta E_{Gap} = 2.86$, 3.27, 3.28, 2.38, 3.08, 3.28, 3.28, and 2.43 eV at PBE0/6–31 + G* level, respectively. Especially, the HOMO-LUMO gap of 3.26 eV obtained for $B_{20}C_{45}$ (**2**) appears to be even larger than the corresponding value of $\Delta E_{Gap} = 3.01$ eV calculated for I_h C_{60} at the same theoretical level, suggesting that these borafullerenes are kinetically stable at room temperature and possible to be synthesized in experiments. As clearly shown in Fig. S5, $B_{20}C_{45}$ (**2**) possesses a similar molecular orbital energy level diagram with C_{60}, with the five degenerate HOMOs (h_u) and three degenerate LUMOs (t_{1u}) orbitals in I_h C_{60} broken into lower degenerate HOMO (e_2) and LUMO (e_1) in C_5 $B_{20}C_{45}$.

We further analyzed the bonding patterns of C_{3v} $B_4C_3H_6$, C_5 $B_{20}C_{45}$ (**2**), and C_{5h} $B_{20}C_{55}$ (**3**) in details using the AdNDP approach which recovers both the localized and delocalized bonds of the concerned systems. As shown in Fig. 3a, the quasi-planar C_{3v} $B_4C_3H_6$ possesses 6 delocalized 3c-2e σ bonds on the B_4C_3 hexagonal framework and 3 totally delocalized 7c-2e π bonds over the bowl-shaped molecular plane, unveiling the aromatic nature of C_{3v} $B_4C_3H_6$ analogous to benzene (C_6H_6) [19]. Figure 3b indicates that $B_{20}C_{45}$ (**2**) possesses 55 2c-2e C–C σ bonds on the top and at the bottom with the occupation numbers of |ON| = 1.93–1.98 |e|, 5 2c-2e C–B σ bonds around the waist between the five isolated B_4C_3-HPs with |ON| = 1.93 |e|, and 30 3c-2e C–B–B σ bonds evenly distributed on the five isolated B_4C_3-HPs with |ON| = 1.96–1.97 |e|. The remaining 60 valence electrons form 30 delocalized π bonds over the σ skeleton, including 15 localized 2c-2e π bonds on the top and bottom with ON = 1.61–

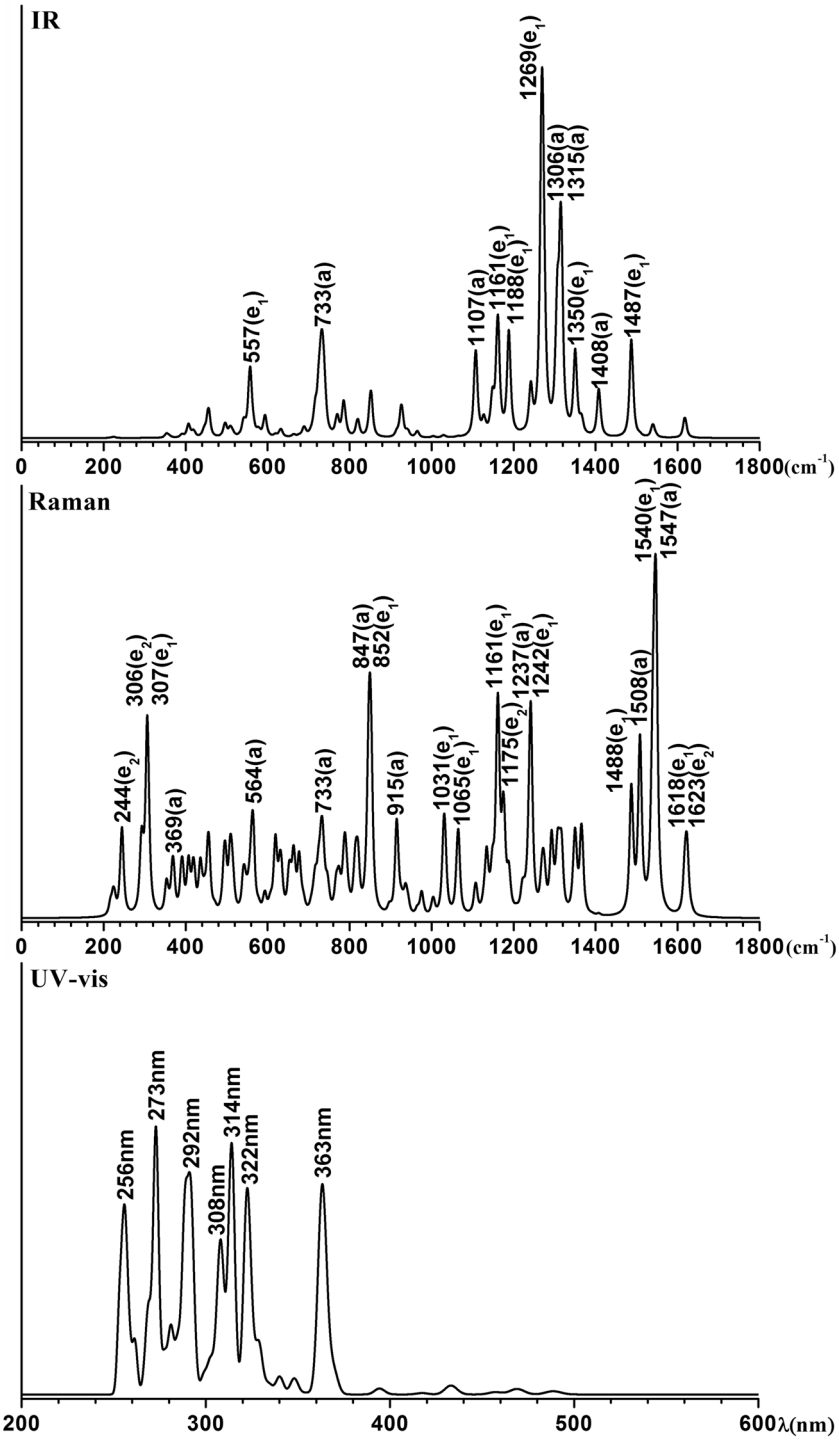

Fig. 4 Simulated **a** IR, **b** Raman, and **c** UV-vis absorption spectra of C_5 $B_{20}C_{45}$ (**2**) at PBE0/6–31 + G(d) level

1.71 |e| and 15 delocalized 7c-2e π bonds evenly distributed over the five isolated B_4C_3-HPs with ON = 1.89–1.96 |e|, in an overall symmetry of C_5. Interestingly, there exist 3 7c-2e π bonds forming a local π-aromatic system over each isolated B_4C_3-HP. The five equivalent B_4C_3-HPs in $B_{20}C_{45}$ (**2**) (Fig. 3b) have therefore well inherited π-bonding patterns of the C_{3v} $B_4C_3H_6$ molecule in Fig. 3a, conferring local π-aromaticity to the borafullerene. Such a bonding pattern exhibits close similarity with that of I_h C_{60} [18]. As shown in Fig. 3c, C_{5h} $B_{20}C_{55}$ (**3**) possesses a similar bonding pattern with $B_{20}C_{45}$ (**2**). It possesses 70 2c-2e C–C σ bonds, 5 2c-2e C–B σ bonds, and 30 3c-2e C–B–B σ bonds in the σ skeleton, over which there exist 20 2c-2e π bonds on the top and bottom and 15 delocalized 7c-2e π bonds over five isolated B_4C_3-HPs around the waist, again with 3 7c-2e π bonds forming an aromatic system over each isolated B_4C_3-HP. Such a bonding

pattern shows close similarity with that of C_{5h} C_{70} [18]. As indicated in Fig. S6, similar AdNDP bonding patterns exist in C_{5h} $B_{20}C_{35}$ (**1**), C_5 $B_{20}C_{65}$ (**4**), S_{10} $B_{40}C_{50}$ (**5**), C_5 $B_{40}C_{60}$ (**6**), S_{10} $B_{40}C_{70}$ (**7**), and C_5 $B_{40}C_{80}$ (**8**). Such bonding patterns render spherical aromaticity to 1–8 borafullerenes, as evidenced by their calculated negative nucleus-independent chemical shifts (NICS) of NICS = − 19, − 16, − 22, − 20, − 16, − 15, − 13, and − 12 ppm at cage center.

Simulated IR, Raman, and UV-vis spectra

Joint infrared photodissociation (IR-PD) spectroscopy and theoretical investigations have proven to be an effective approach in characterizing novel clusters in gas phases [41, 42]. The IR and Raman spectra of the prototypical C_5 $B_{20}C_{45}$ (**2**) are simulated in Fig. 4. It exhibits major IR active peaks at 557 (e_1), 733 (a), 1161 (e_1), 1269 (e_1), 1315 (a), and 1487(e_1) cm^{-1} and Raman active peaks at 306 (e_2), 847 (a), 1161 (e_1), 1237 (a), and 1540 (e_1) cm^{-1}, respectively. The Raman vibration at 369 cm^{-1} originates from typical radial breathing mode (a) of the cage-like $B_{20}C_{45}$ (**2**) which may be used to characterize boron-containing hollow nanostructures [43].

The simulated UV-vis spectrum of $B_{20}C_{45}$ (**2**) exhibits strong absorption peaks at 256, 273, 292, 314, 322, and 363 nm, respectively (Fig. 4). These strong UV absorptions mainly originate from electron transitions from the deep inner shells to the highly unoccupied molecular orbitals of $B_{20}C_{45}$ (**2**), while the weak UV-vis absorptions above 400 nm correspond to electronic excitations from the occupied frontier orbitals (HOMO and HOMO-1) to the unoccupied frontier orbitals of the system (LUMO, LUMO+1, and LUMO+2) (Fig. 4).

Conclusions

In summary, based on extensive first-principles theory calculations, we have predicted in this work a series of spherically aromatic borafullerenes $B_{20}C_{35}$ (**1**), $B_{20}C_{45}$ (**2**), $B_{20}C_{55}$ (**3**), $B_{20}C_{65}$ (**4**), $B_{40}C_{50}$ (**5**), $B_{40}C_{60}$ (**6**), $B_{40}C_{70}$ (**7**), and $B_{40}C_{80}$ (**8**) at DFT level which all follow the IHPR rule via isovalent substitutions from their fullerene analogues. The isovalent substitution strategy developed in [19] and this work and the structural and bonding patterns demonstrated in boragraphenes and borafullerenes may be applied to form other heterographenes and heterofullerenes with promising properties to develop novel nanodevices.

Funding information This work was supported by the National Natural Science Foundation of China (21720102006 and 21973057 to S.-D. Li, 21903049 to X.-X. Tian, 21803037 to W.-Y. Zan and 11504213 to Y.-W. Mu).

References

1. Kroto HW (1987) The stability of the fullerenes C_n, with n = 24, 28, 32, 36, 50, 60 and 70. Nature (London, United Kingdom) 329:529–531. https://doi.org/10.1038/329529a0
2. Schmalz TG, Seitz WA, Klein DJ, Hite GE (1988) Elemental carbon cages. J. Am. Chem. Soc. 110:1113–1127. https://doi.org/10.1021/ja00212a020
3. Kroto HW, Heath JR, O'Brien SC, Curl RF, Smalley RE (1985) C_{60}: buckminsterfullerene. Nature 318:162–163. https://doi.org/10.1038/318162a0
4. Lamparth I, Nuber B, Schick G, Skiebe A, Grösser T, Hirsch A (1995) $C_{59}N^+$ and $C_{69}N^+$: isoelectronic heteroanalogues of C_{60} and C_{70}. Angew. Chem. 107: 2473-2476. https://doi.org/10.1002/ange.19951072035; Angew. Chem. Int. Ed. Engl. 34: 2257–2259. https://doi.org/10.1002/anie.199522571
5. Nuber B, Hirsch A (1996) A new route to nitrogen heterofullerenes and the first synthesis of $(C_{69}N)_2$. Chem. Commun. 12:1421–1422. https://doi.org/10.1039/cc9960001421
6. Guo T, Jin CM, Smalley RE (1991) Doping bucky: formation and properties of boron-doped buckminsterfullerene. J. Phys. Chem. 95:4948–4950. https://doi.org/10.1021/j100166a010
7. Kimura T, Sugai T, Shinohara H (1996) Production and characterization of boron- and silicon-doped carbon clusters. Chem. Phys. Lett. 256:269–273. https://doi.org/10.1016/0009-2614(96)00436-8
8. Muhr HJ, Nesper R, Schnyder B, Kötz R (1996) The boron heterofullerenes $C_{59}B$ and $C_{69}B$: generation, extraction, mass spectrometric and XPS characterization. Chem. Phys. Lett. 249:399–405. https://doi.org/10.1016/0009-2614(95)01451-9
9. Dunk PW, Rodríguez-Fortea A, Kaiser NK, Shinohara H, Poblet JM, Kroto HW (2013) Formation of heterofullerenes by direct exposure of C_{60} to boron vapor. Angew. Chem. Int. Ed. 52:315–319. https://doi.org/10.1002/anie.201208244
10. Kurita N, Kobayashi K, Kumahora H, Tago K, Ozawa K (1992) Molecular structures, binding energies and electronic properties of dopyballs $C_{59}X$ (X= B, N and S). Chem. Phys. Lett. 198:95–99. https://doi.org/10.1016/0009-2614(92)90054-Q
11. Kurita N, Kobayashi K, Kumahora H, Tago K (1993) Bonding and electronic properties of substituted fullerenes $C_{58}B_2$ and $C_{58}N_2$. Phys. Rev. B 48:4850–4854. https://doi.org/10.1080/15363839308011901
12. Miyamoto Y, Hamada N, Oshiyama A, Saito S (1992) Electronic structures of solid BC_{59}. Phys. Rev. B 46:1749–1753. https://doi.org/10.1103/PhysRevB.46.1749
13. Zou Y, Luo MX, Wang ZJ, Li WZ (1998) Properties of boron-substituted heterofullerenes. Chin. Phys. Lett. 15:106–108. https://doi.org/10.1088/0256-307X/15/2/011
14. Chen ZF, Zhao XZ, Tang A (1999) Theoretical studies of the substitution patterns in heterofullerenes $C_{60-x}N_x$ and $C_{60-x}B_x$ (x=2-8). J. Phys. Chem. A 103:10961–10968. https://doi.org/10.1021/jp9908707
15. Xie RH, Jensen L, Bryant GW, Zhao JJ, Smith Jr VH (2003) Structural, electronic, and magnetic properties of heterofullerene $C_{48}B_{12}$. Chem. Phys. Lett. 375:445–451. https://doi.org/10.1016/S0009-2614(03)00879-0
16. Garg I, Sharma H, Dharamvir K, Jindal VK (2011) Substitutional patterns in boron doped heterofullerenes $C_{60-n}B_n$ (n = 1–12). J. Comput. Theor. Nanosci. 8:642–655. https://doi.org/10.1166/jctn.2011.1734
17. Mohr S, Pochet P, Amsler M, Schaefer B, Sadeghi A, Genovese L, Goedecker S (2014) Boron aggregation in the ground states of boron-carbon fullerenes. Phys. Rev. B 89:041404(R). https://doi.org/10.1103/PhysRevB.89.041404

18. Yan M, Tian XX, Pei L, Li SD (2018) Cage-like $B_{40}C_{30}$, $B_{40}C_{40}$, and $B_{40}C_{50}$: high-symmetry heterofullerenes isovalent with C_{60}, C_{70}, and C_{80}. J. Mol. Model. 24:296. https://doi.org/10.1007/s00894-018-3828-z
19. Tian XX, Xuan XY, Yu M, Mu YW, Lu HG, Zhang ZH, Li SD (2019) Predicting two-dimensional semiconducting boron carbides. Nanoscale 11:11099–11106. https://doi.org/10.1039/c9nr02681a
20. Chen X, Zhao YF, Wang LS, Li J (2017) Recent progresses of global minimum searches of nanoclusters with a constrained basin-hopping algorithm in the TGMin program. Comput. Theor. Chem. 1107:57–65. https://doi.org/10.1016/j.comptc.2016.12.028
21. Zhao YF, Chen X, Li J (2017) TGMin: a global-minimum structure search program based on a constrained basin-hopping algorithm. Nano. Res. 10:3407–3420. https://doi.org/10.1007/s12274-017-1553-z
22. Chen X, Zhao YF, Zhang YY, Li J (2019) TGMin: an efficient global minimum searching program for free and surface-supported clusters. J. Comput. Chem. 40:1105–1112. https://doi.org/10.1002/jcc.25649
23. Goedecker S, Hellmann W, Lenosky T (2005) Global minimum determination of the Born-Oppenheimer surface within density functional theory. Phys. Rev. Lett. 95:055501. https://doi.org/10.1103/PhysRevLett.95.055501
24. Goedecker S (2004) Minima hopping: an efficient search method for the global minimum of the potential energy surface of complex molecular systems. J. Chem. Phys. 120:9911–9917. https://doi.org/10.1063/1.1724816
25. Adamo C, Barone V (1999) Toward reliable density functional methods without adjustable parameters: the PBE0 model. J. Chem. Phys. 110:6158–6170. https://doi.org/10.1063/1.478522
26. Krishnan R, Binkley JS, Seeger R, Pople JA (1980) Self-consistent molecular orbital methods. XX. A basis set for correlated wave functions. J. Chem. Phys. 72:650–654. https://doi.org/10.1063/1.438955
27. Zhai HJ, Zhao YF, Li WL, Chen Q, Bai H, Hu HS, Piazza ZA, Tian WJ, Lu HG, Wu YB, Mu YW, Wei GF, Liu ZP, Li J, Li SD, Wang LS (2014) Observation of an all-boron fullerene. Nat. Chem. 6:727–731. https://doi.org/10.1038/nchem.1999
28. Chen Q, Li WL, Zhao YF, Zhang SY, Hu HS, Bai H, Li HR, Tian WJ, Lu HG, Zhai HJ, Li SD, Li J, Wang LS (2015) Experimental and theoretical evidence of an axially chiral borospherene. ACS. Nano. 9:754–760. https://doi.org/10.1021/nn506262c
29. Chen Q, Zhang SY, Bai H, Tian WJ, Gao T, Li HR, Miao CQ, Mu YW, Lu HG, Zhai HJ, Li SD (2015) Cage-like B_{41}^{+} and B_{42}^{2+}: new chiral members of the borospherene family. Angew. Chem. Int. Ed. 54:8160–8164. https://doi.org/10.1002/anie.201501588
30. Wang LS (2016) Photoelectron spectroscopy of size-selected boron clusters: from planar structures to borophenes and borospherenes. Int. Rev. Phys. Chem. 35:69–142. https://doi.org/10.1080/0144235X.2016.1147816
31. Jian T, Chen XN, Li SD, Boldyrev AI, Li J, Wang LS (2019) Probing the structures and bonding of size-selected boron and doped-boron clusters. Chem. Soc. Rev. 48:3550–3591. https://doi.org/10.1039/c9cs00233b
32. Zubarev DY, Boldyrev AI (2008) Developing paradigms of chemical bonding: adaptive natural density partitioning. Phys. Chem. Chem. Phys. 10:5207–5217. https://doi.org/10.1039/b804083d
33. Zubarev DY, Boldyrev AI (2008) Revealing intuitively assessable chemical bonding patterns in organic aromatic molecules via adaptive natural density partitioning. J. Org. Chem. 73:9251–9258. https://doi.org/10.1021/jo801407e
34. Tkachenko NV, Boldyrev AI (2019) Chemical bonding analysis of excited states using the adaptive natural density partitioning method. Phys. Chem. Chem. Phys. 21:9590–9596. https://doi.org/10.1039/c9cp00379g
35. Schleyer PvR, Maerker C, Dransfeld A, Jiao HJ, van Eikema Hommes NJR (1996) Nucleus-independent chemical shifts: a simple and efficient aromaticity probe. J. Am. Chem. Soc. 118:6317–6318. https://doi.org/10.1021/JA960582D
36. Chen ZF, Wannere CS, Corminboeuf C, Puchta R, Schleyer PvR (2005) Nucleus-independent chemical shifts (NICS) as an aromaticity criterion. Chem. Rev. 105:3842–3888. https://doi.org/10.1021/cr030088+
37. Bauernschmitt R, Ahlrichs R (1996) Treatment of electronic excitations within the adiabatic approximation of time dependent density functional theory. Chem. Phys. Lett. 256:454–464. https://doi.org/10.1016/0009-2614(96)00440-X
38. Casida ME, Jamorski C, Casida KC, Salahub DR (1998) Molecular excitation energies to high-lying bound states from time-dependent density-functional response theory: characterization and correction of the time-dependent local density approximation ionization threshold. J. Chem. Phys. 108:4439–4449. https://doi.org/10.1063/1.475855
39. VandeVondele J, Krack M, Mohamed F, Parrinello M, Chassaing T, Hutter J (2005) QUICKSTEP: fast and accurate density functional calculations using a mixed Gaussian and plane waves approach. Comput. Phys. Commun. 167:103–128. https://doi.org/10.1016/j.cpc.2004.12.014
40. Frisch MJ, Trucks GW, Schlegel HB, Scuseria GE, Robb MA, Cheeseman JR, Scalmani G, Barone V, Mennucci B, Petersson GA et al (2009) Gaussian 09, revision D.01. Gaussian, Inc., Wallingford
41. Wang GJ, Zhou MF, Goettel JT, Schrobilgen GJ, Su J, Li J, Schlöder T, Riedel S (2014) Identification of an iridium-containing compound with a formal oxidation state of IX. Nature 514:475–477. https://doi.org/10.1038/nature13795
42. Fagiani MR, Song XW, Petkov P, Debnath S, Gewinner S, Schöllkopf W, Heine T (2017) Untersuchung der struktur und dynamik des B_{13}^{+} mithilfe der Infrarot-p hotodissoziationsspektroskopie. Angew. Chem. 129:515–519. https://doi.org/10.1002/ange.201609766
43. Ciuparu D, Klie RF, Zhu YM, Pfefferle L (2004) Synthesis of pure boron single-wall nanotubes. J. Phys. Chem. B 108:3967–3969. https://doi.org/10.1021/jp049301b